Effect on Fatigue Behavior of Connecting Rod in Gasoline Engine

Yodnapha Ketmuang

Automotive Manufacturing Engineering Department, Faculty of Engineering and Technology, Panyapiwat Institute of Management, Thailand
yodnaphaket@pim.ac.th

Bundit Wongthong

Department of Industrial Engineering, Faculty of Engineering, Thonburi University, Thailand
bundid.w@gmail.com (corresponding author)

ABSTRACT

This article reports the failure analysis of a connecting rod that is broken into 3 pieces and is used in the gasoline engine of a sedan. The connecting rod is made of JIS-S50C medium alloyed steel. Fractography was performed to characterize the failure mode on the fracture surface of this connecting rod through the examination of the macroscopic and microscopic morphologies of the fracture surface, chemical composition, metallographic analysis, mechanical properties of the material, and numerical simulation. The fracture surface of this connecting rod is caused by fatigue, which was the dominant mechanism of failure. This type of crack is indicative of shear failure in the ductile fracture mode, whereas no abnormalities were found in the composite elements of the connecting rod. The microstructure is composed of perlite-ferrite. The results of the numerical simulation and the calculated crushing stress (s_c) were compared and were found to be in accordance and within the acceptable values.

Keywords-connecting rod; JIS-S55C; fracture surface; fatigue; numerical simulation

I. INTRODUCTION

The connecting rod is an important component of a gasoline engine. It consists of three main parts: The piston pin end, the center shank, and the big end, as shown in Figure 1. The piston pin end is the small end, the crank pin end is the big end, and the center shank is of I-cross section [1].

The design of the shank can be of different types, e.g., rectangular, tubular, circular, I-section and H-section. The circular section is generally used for low-speed engines, whereas the I-section is utilized for high-speed engines [2]. The connecting rod manufacturing processes are included in Figure 2. Casting, also known as sand molded casting, is a metal casting process characterized by the employment of sand as the mold material. The term "sand casting" can also refer to an object produced via the casting process through which over 70% of all metal castings are constructed. Forging is a manufacturing process involving the shaping of metal deploying localized compressive forces. Forging is often classified according to the temperature at which it is performed: "cold", "warm", or "hot" forging. Machining is best executed with the alloy steel JIS-S50C in annealed or normalized and tempered condition. It can be readily machined by all conventional methods, such as sawing, turning, drilling etc. The Powder forging process offers advantages, involving reduced material waste, elimination of re-heating steps, and lower temperature requirements compared to the conventional forging. This process is particularly suitable for manufacturing connecting rods that require high strength and durability. The accuracy of parts must be maintained despite wide daily and seasonal shop floor temperature ranges. With fluctuations in some environments varying over 20 °C, thermal growth and its effects need to be taken into consideration. Current gauges provide simple pass/ fail results and it is thus difficult to accurately record inspection data, determine how close a feature is to the tolerance, and have the necessary data to improve process control [3].

Regarding the applications, the connecting rod is utilized to support the reverse and alternating rotation, so the connecting rod must be strong and durable in the long term for the use of that vehicle. Concerning the failure of the connecting rods, authors in [4] investigate two case studies on the failure of truck diesel engine connecting-rods. Fatigue is the dominant failure mode of the two connecting rods. The occurrence of an abnormal load in operation and the presence of a thick decarburization layer on the external surface of the rod body are, respectively, responsible for the fatigue failure of the two connecting rods [4].
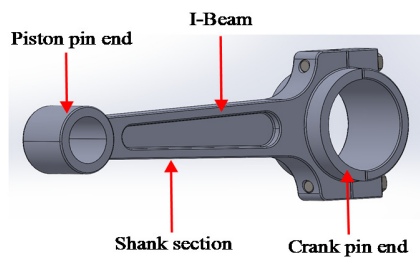
Fig. 1.   Components of the connecting rod.

Fig. 2.   The manufacturing of the connecting rods.

A failure analysis investigation carried out on a connecting rod from a diesel engine used to generate electrical energy, found that the connecting rod broke in a section close to the head [5]. The origin of the fracture was located at the con-rod lubrication channel. The lubrication channel exhibited an area containing a tungsten-based material, presumably from a machining tool, embedded in its surface due to an incomplete manufacturing process. This area acted as a nucleation site for cracks that propagated through the connecting rod section by a fatigue mechanism, reducing its section and ultimately causing its catastrophic failure [5]. Authors in [6] conducted a thorough fatigue failure analysis of the diesel engine connecting rod. This investigation suggested that the latter failed due to improper machining/ drilling of the oil hole and chamfer on the small end of the connecting rod, which had generated rough tool marks in the inner diameter, serration marks and material chip off. These induced harmful residual tensile stresses resulting in early fatigue failure [6]. An analysis of the failure-split performance of 36MnVS4 detected defects [7]. To investigate the causes of defects that occurred, the material properties and fracture-split performance of the 36MnVS4 are researched and compared with C70S6. The fracture-split easily induced defects are also analyzed. By finite element simulation and experimental analysis, the results manifest that the 36MnVS4 has lower carbon content and more ferrite, therefore the fracture surface of the 36MnVS4 connecting rod is more prone to tear and the plastic deformation range is greater. By altering the cross-section design, the outer edge of the joint surface is changed into an arc-shape, which can improve the fracture-split process of the 36MnVS4 connecting rod and reduce the processing defects [7]. According to [8], the main cause of damage is fatigue. It was also found that the beginning of the crack was generated by corrosion or a defect in the material. It was concluded that the main cause of the connecting rod damage was the high stress levels in the vicinity of the bolt holes, provoked by the very high tightening force of the bolts [8]. Researchers in [9], investigated the failure of the connecting rod of a 1.5 dci K9K diesel engine. As a result of the engine operating for approximately 378400 km, the connecting rod was broken, and the reasons for the failure of the connecting rod cap and connecting bolt were investigated. According to the numerical analysis results, with the increase of the tightening torque, the maximum equivalent stress and

alternating stress values increased significantly, whereas the fatigue safety factor and the cycle of life of the connecting rod decreased. Authors in [10] determined the origin, velocity, and the duration of the fatigue crack development of a diesel alternator engine, which suffered a significant failure of one of its parts, not long after a major overhaul had been completed and with less than 1000 running hours having elapsed. The results were verified by the fatigue rupture of one of the four connecting rod stud bolts. Tensile tests were performed on the remaining connecting rod bolts. During this process, another fatigue crack was identified in an adjacent bolt. The probable root case of damage and some final remarks are presented. Authors in [11] determined that the damage on the connecting rod was caused by a compression leak due to cylinder wear. SEM analysis revealed that the piston core material was discolored due to heat, namely the formation of iron oxide. The level of heat experienced by the connecting rod was approximately 200 °C and EDX analysis suggested high levels of iron (Fe) and oxygen (O), confirming that the formation of iron oxide on the metal surface is caused by the influence of heat [11]. In [12], the authors adjusted the connecting rod structure. The mass of the connecting rod was reduced by 5.85%, the maximum stress was decreased by 13.7%, and the safety factor was increased by 16.0%. By studying the effect of the cross-section parameters of the rod body and the large end transition fillet on the connecting rod stress, an empirical formula for calculating the maximum stress of the connecting rod was adapted for this model and similar types. Technology design provided a new analysis method, improved the efficiency of structural optimization and strength analysis of the connecting rod assembly. The former also filled the research gap of strength analysis and structural optimization of the low-speed diesel engine connecting rod [12].

This research aims to study connecting rod failure by different test and analysis methods. Additionally, finite element analysis can indicate the influence of stress on the mechanical part, providing insights that can effectively guide limiting transmission power to ensure extended service life.

II.   EXPERIMENTAL PROCEDURE

For the identification of the cause of the failure several experiments with the connecting rod were required. Initially the geometric dimensions were measured with a 3D coordinate measuring machine. The failed connecting rod had to be examined macroscopically to get the overall picture, with images of the general characteristics of the fracture surface captured on a digital camera (Nikon D80). The fracture surface was then subjected to more detailed microscopic examinations using a scanning electron microscope (JEOL: JSM-7800F prime). Secondly, a material inspection was conducted to determine the chemical analysis and metallurgical structure with the requirements of the failed connecting rod material. The chemical analysis of the failed connecting rod material was determined deploying an optical emission spectrometer (Thermo: ARL 3460). The metallographic examination of the failed connecting rod was photographed utilizing an optical microscope (Olympus laser microscopes: OLS 4000). Furthermore, a mechanical property test was performed, measuring the micro-hardness using an ANTON PAAR: MHT-

10 with a diamond indentation with a pyramidal angle of $136°$ and pressing load of 300 g. The purpose of this test was to create a hardness profile from the surface through the central axis and align the indentation to the other surface, to one side of the connecting rod near the surface area of the fracture surface.

Numerical finite elements' stress analysis was performed implementing the ANSYS Workbench simulator. The software used linear equations that govern the motion behavior of the x, y and z axis, parameters related to the numerical simulation. ANSYS Workbench is a software applied to analyze the bending and torsional moments in the connecting rod structures. The resulting geometry from the Solid work program will be the initial one obtained from the connecting rod. After that, the finite element model was determined from the relevant parameters. The problem analysis and verification results are critical factors that occur in the connecting rod under load that can be summarized for use in conjunction with the technical analysis acquired from the experiment.

III. RESULTS AND DISCUSSION

A. Chemical Composition

The chemical composition of the connecting rod material was analyzed using a spectrophotometer test machine. The average values of the chemical composition of connecting rod material are portrayed in Table I. The field connecting rod chemical compositions are made from medium-alloyed steels JIS -S50C, which are commonly and widely used in connecting rod manufacturing [13].

TABLE I.   CHEMICAL COMPOSITION OF THE FIALED CONNECTING ROD AND THOSE JIS-S50C STEELS (WT.%).

Material	Failed connecting rod	S50C [14]
C	0.527	0.47-0.55
Si	0.260	0.15-0.35
Mn	0.901	0.60-0.90
P	0.003	≤ 0.035
S	0.054	≤ 0.035
Ni	0.0057	≤ 0.25
Cr	0.0468	≤ 0.25

B. Visual Inspection

The visual examination of the failed connecting rod in Figure 3 indicates that there are 3 damaged parts. The first connecting rod has a broken surface and the entire surface is abrasive, as shown in Figure 4. The second connecting rod has a relatively intact surface, as noticed in Figure 5, which displays the starting point of the crack origin appearing at multiple points. The crack slowly expands through the fatigue zone, or the damaged area by periodic loading. During the slow crack propagation there are variations in the applied force, affecting the crack growth rate. When the crack expands for a while, the material has little space to support the force and causes an area to receive the final overload. In that area, it was found that most of the cracks that expanded were macroscopically characterized as brittle fractures. In the third connecting rod, the fracture surface is partially rubbed and there are signs of broken surface, as observed in Figure 6 [8].

Fig. 3.   The connecting rod is broken into 3 pieces.
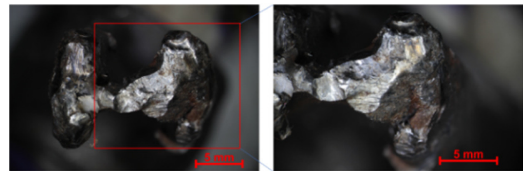

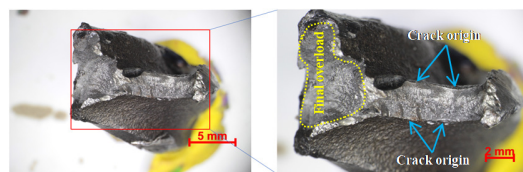Fig. 4.   Surface of the first connecting rod.

Fig. 5.   Broken surface of the second connecting rod.

Fig. 6.   Broken surface of the third connecting rod.

C. SEM and EDX Analysis

Examining the fracture in the second failed connecting rod by using a scanning electron microscope, a close- up image of the final overload fracture in the connecting rod is detected in Figure 7(a). Dimples are clearly apparent from the same point in Figure 7(b) when it is magnified. This structure is characteristic of a fracture followed on by uniaxial tensile failure. Each dimple is one half of a micro void formed during the fracture process and is subsequently cracked separately. In case of fracture, dimples appear on the 45-degree shear lip. The ductile fracture form, resulting from the shear behavior, is elongated or C-shaped, and this parabolic shape may be characteristic of shear failure [11, 14]. Figure 7(c) depicts a surface layer examination of the same area. SEM was deployed to analyze the chemical composition of the fracture surfaces of the failed connecting rod for inclusions using energy dispersive spectroscopy (EDS). The line of scan discloses that most elements within the standard weight percentage of steel material are iron (Fe), carbon (C), and manganese (Mn). Connecting rod alloy composition is confirmed to be medium alloy S50C with no abnormalities.
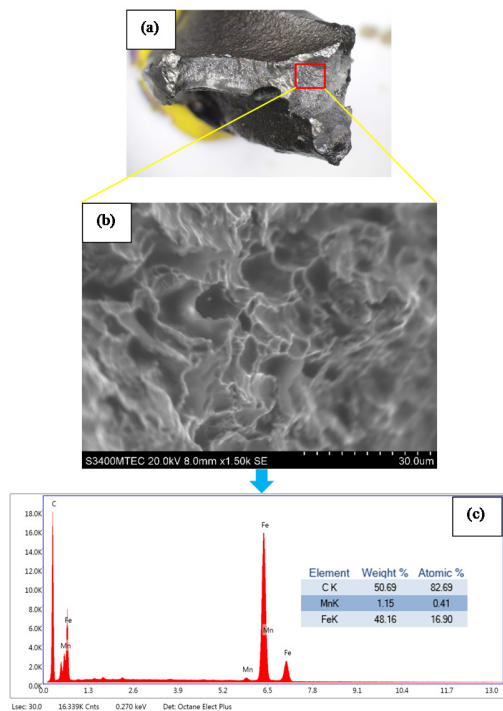
Fig. 7.   (a) The final overload fracture. (b) Dimples at a magnification of 1.5kx. 30 μm. (c) The EDS results on the final overload zone from the same areas.
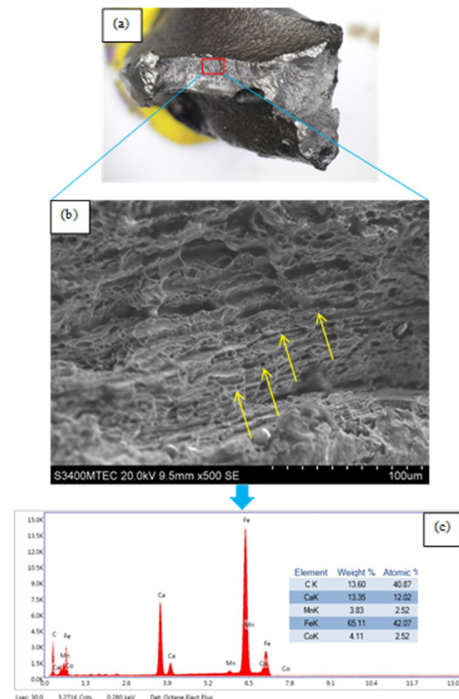

Fig. 8.   (a) SEM micrograph showing 1x. (b) Magnification of the visible fracture area demonstrating fatigue striations and the direction of motion between dislocations of atoms. (c) EDS results on the fracture zone from the same areas.

The photograph at the surface region in Figure 8 (a) is a magnified image of the surface fracture area of the connecting rod. An enlarged section exhibiting fatigue striations and revealing the displacement direction between atoms, with fatigue striations in each stress period or each stress cycle acting on the specimen is observed in Figure 8 (b). These lines can only be seen through examination by a high-powered microscope. Figure 8 (c) depicts a surface layer examination of the same area. SEM was used to analyze the chemical composition of the fracture surfaces of the failed connecting rod for inclusions implementing EDS. The line of scan reveals that most elements within the standard percentage by weight of steel material are iron (Fe), carbon (C), Calcium (Ca), manganese (Mn) and (Co) Cobalt. The connecting rod alloy composition was confirmed to be medium alloy S50C with no abnormalities.

D. Microstructure Analysis

Metallographic examinations were also performed. A transverse cross section of the failed connecting rod was cold mounted using epoxy resin, then ground using emery paper (down to #1200 grit) and polished with 1 μm diamond paste. The microstructure was etched by using 2% nital solution (2 ml HNO_3 + 100 ml DI water) and examined using light optical microscope (OM). Figure 9(a) shows a low magnification image (1x) with two telescopes at the surface and core of the connecting rod. The central axis in Figure 9(b) contains a perlite-ferrite microstructure and found manganese sulfite inserted in the ground metal. The cross-section and microstructure of the outer surface showed pearlite-ferrite in Figure 9(c).
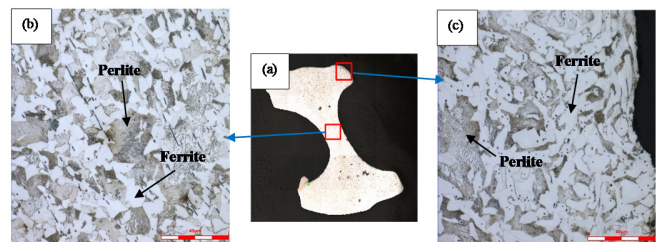

Fig. 9.   Microstructure of the connecting rod (a) Photograph taken at low power 1x. (b) Photograph of the microstructure center consisting of pearlite-ferrite. (c) Photograph of the microstructure surface with Pearlite-ferrite composition.

E. Hardness Measurement

A connecting rod hardness testing by Vickers hardness measurement using an Anton Paar hardness tester: MHT-10 was performed. The cross-sectional hardness measurement employs a pyramid-shaped diamond indenter with a square base with an angle of 136° starting from the outer surface of the connecting rod into the core of the connecting rod at all 12 points. The results of the hardness measurement were obtained. As portrayed in Figure 10, the maximum hardness at the connecting rod surface is 324 HV. The hardness decreases along the radial direction (0.45 mm) until the minimum hardness at the center of the shaft is 261 HV [4, 14].

F. Stress Analysis using Numerical Simulation.

The material deployed in the study was a failed connecting rod obtained from a sedan produced in 2012. The connecting

rod was made of JIS-S50C grade medium carbon steel. The technical data of this car model are shown in Table II.
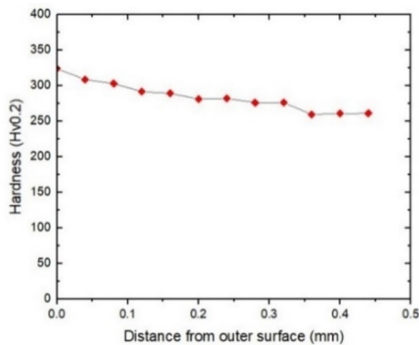

Fig. 10.   Hardness graph measured from the outer surface edge to the center of the connecting rod.

TABLE II.   ENGINE SPECIFICATIONS

Item	Specifications
Piston displacement	660 cc.
Bore x Stroke	63.0 x 70.4
Compression ratio	11.3 : 1
Maximum Power	52 Hp / 6,800 rpm
Maximum Torque	60 N-m / 5,200 rpm
Maximum pressure	25 MPa

A structural analysis of the connecting rod was performed with the Ansys program. A theoretical static analysis of the steel material connecting rod was carried out [15]. The crushing stress (σ_c) can be analyzed by the (1) [16].

$$\sigma_c = \frac{F_P FOS}{2A} \qquad (1)$$

where F_p is the gas force of piston top (77,931 N), F_r is the inertia force of the reciprocating parts (3529 N), F_f is the friction force between the piston and cylinder wall, which can be neglected, because it reduces the applied force on the connecting rod, W is the force generated due to the weight of reciprocating mass (9.42 N), A is the area of the piston pin subjected to double shear stress (159 mm^2). FP is the force on the piston pin that can be found by (2) [17]:

$$F_P = F_g - F_r \pm F_f + W \qquad (2)$$

$$F_P = 77,931 - 3529 + 9.42 = 74,411.42$$

The crushing stress (σ_c) can be found from

$$\sigma_c = \frac{74411.42 \times 3}{2 \times 159} = 702 \text{N/m}^2$$

The stress analysis using the finite element method in the piston pin subjected to crushing stress was calculated according to the design criteria. A 3D scanner was utilized to measure the shape of the connecting rod, to convert it into the Solid Works 2018 program and put it into a numerical simulation in the Ansys Workbench program as shown in Figure 11.
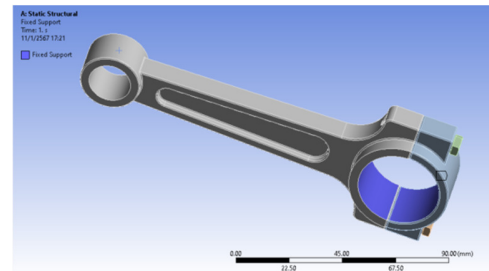

Fig. 11.   Three-dimensional model of the connecting rod obtained from converting Solid work into Ansys Workbench.

The connecting rod mesh adjustment was performed using a torque value of 60 N-m (obtained from the repair manual of this model), the mechanical properties of the connecting rod material were explored using a Young's modulus value of 210G Pa, density of 7.85 g/ cm3 and Poisson's ratio of 0.3 [13]. Mesh (Mesh) is generated with tetrahedral elements as manifested in Figure 12. The generated mesh functional model has a total of 25,646 elements, and a total of 36,762 nodes are selected for mesh control. Each node has a DOF of 5,404 moves only in the x, y, and z directions [18]. The analysis was applied to a connecting rod subjected to torque. After that, the stress distribution was obtained as a number and imported into the Ansys Workbench program, as demonstrated in Figure 13. The Equivalent von Mises stress max value is 645.37 MPa. Figure 14 exhibits the total deformation max value, which is 0.50017 mm, Figure 15 presents the endurance limits max value, which is 106 cycles and Figure 16 provides the safety factor max value [16-25].
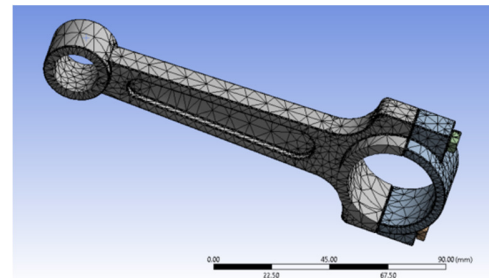

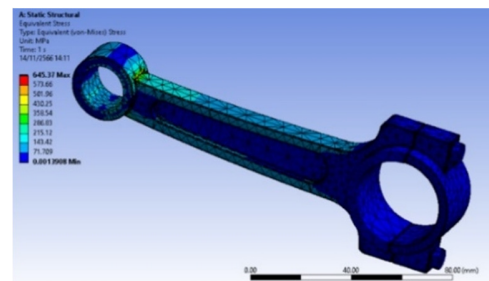Fig. 12.   Mesh obtained from numerical monkey simulation.

Fig. 13.   Von mises stress values obtained from numerical simulations.

The calculated crushing stress (σ_c) was 702 MPa, and the numerical simulation results of Ansys Workbench were 645.37 MPa. The results differed by no more than 8%, which ensured

that the program was not compromised. The yield strength of the material is 415M Pa [16-25]. The calculated stress value is 1.69 times greater than the yield strength, which results in the final shaft fracture. In conclusion, if the stress is greater than the yield strength which the material can support, this is the cause of the connecting rod breaking [16-24].
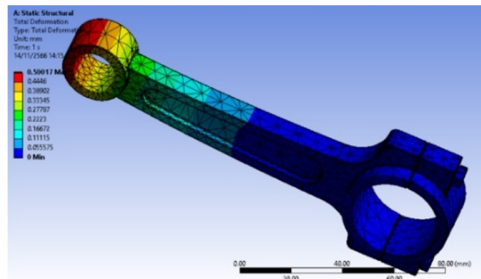

Fig. 14.   Total deformation values obtained from numerical simulations.
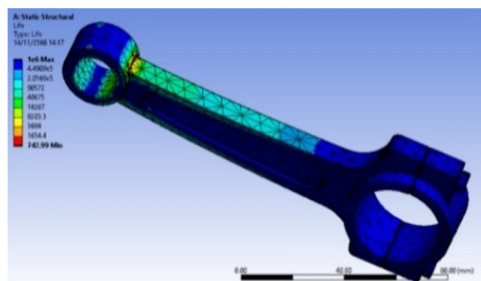

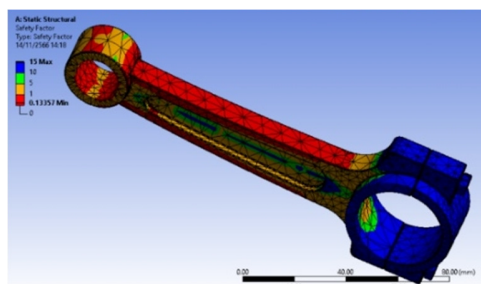Fig. 15.   Fatigue endurance limit values obtained from numerical simulations.

Fig. 16.   Safety factor obtained from numerical simulations.

IV.   CONCLUSION

This research was conducted on a failed connecting rod used in a sedan. Based on the results and the analysis presented in this research, the following conclusions can be drawn from the investigation:

A fractography examination on the fracture surface of the connecting rod was conducted. The beginning of the crack origins that occur in multiple points are then propagated to the instant fracture zone, attributed to the high intensity of the stress exerted on the workpiece. This led to a substantial final overload zone. The difference between the results of the numerical simulation and the calculation of the stress value is 8%, which is within the acceptable value. Also, the calculated stress of the material is 702 MPa. The calculated stress value is 1.69 times greater than the yield strength, which may be part of the cause of the connecting rod breakage.

According to the experimental research and simulation model, it can be concluded that excessive stress leads to fracture in the connecting rod. The simulation model examined/developed through a software program is used to identify the root cause of failure for the vehicle component, which led to limited working operation or identified service life.

This case study suggests that the surface hardening process should be improved so that the outer surface of the connecting rod has a martensite microstructure to enhance strength.

REFERENCES

[1] M. Atharuddin, J. A. Sandeep Kumar, P. Hussain, M. Reddy, "Design & Analysis of a Connecting Rod with Different Materials," *Journal of Engineering Sciences*, vol. 10, no. 11, pp. 184-196, Nov. 2019.

[2] D. Aawnre, A. Pratap Singh, "A-Review Paper and Parameter Discussion on Connecting Rod," *International Journal of Research Publication and Reviews*, vol. 4, no. 6, pp. 2472-2475, Jun. 2023.

[3] A. Kar, "Connecting Rod Mannufacturing," Czech Technical University in Prague, MAE2018TAP, Jan. 2019.

[4] Z. Yu and X. Xu, "Fatigue Fracture of Truck Diesel Engine Connecting-Rods," *Journal of Failure Analysis and Prevention*, vol. 15, no. 2, pp. 311–319, Apr. 2015, https://doi.org/10.1007/s11668-015-9934-7.

[5] C. Juarez, F. Rumiche, A. Rozas, J. Cuisano, and P. Lean, "Failure analysis of a diesel generator connecting rod," *Case Studies in Engineering Failure Analysis*, vol. 7, pp. 24–31, Oct. 2016, https://doi.org/10.1016/j.csefa.2016.06.001.

[6] M. T. Alam, A. Thakur, V. Ps. Kumar, and S. Ghadei, "Fatigue Failure Analysis of Diesel Engine Connecting Rod," presented at the International Conference on Advances in Design, Materials, Manufacturing and Surface Engineering for Mobility, Jul. 2018, pp. 2018-28–0067, https://doi.org/10.4271/2018-28-0067.

[7] Z. Shi and S. Kou, "Study on Fracture-Split Performance of 36MnVS4 and Analysis of Fracture-Split Easily-Induced Defects," *Metals*, vol. 8, no. 9, Sep. 2018, Art. no. 696, https://doi.org/10.3390/met8090696.

[8] L. Witek, "Failure and thermo-mechanical stress analysis of the exhaust valve of diesel engine," *Engineering Failure Analysis*, vol. 66, pp. 154-165, Aug. 2016, https://doi.org/10.1016/j.engfailanal.2016.04.022.

[9] M. Guven Gok, O. Cihan, "Investigation of Failure Mechanism of a DCI Engine Connecting Rod," *European Journal of Technique*, vol. 11, no. 2, pp. 374-382, Sep. 2021, https://doi.org/10.36222/ejt.957287.

[10] K. Carjova, V. Priednieks, R. Klaucans, I. Irbe, and A. Urbahs, "Fractographic Study of Marine Diesel Engine Connecting Rod Stud Bolt Crack," *Latvian Journal of Physics and Technical Sciences*, vol. 58, no. 4, pp. 28–42, Aug. 2021, https://doi.org/10.2478/lpts-2021-0031.

[11] W. Wilarso, C. W. M. Noor, A. F. M. Ayob, and W. N. W. Mansor, "Investigation and failure analysis of a diesel generator connecting rod," *Mechanical Engineering for Society and Industry*, vol. 2, no. 2, pp. 64–71, May 2022, https://doi.org/10.31603/mesi.66242.

[12] W. Gao, G. Wang, J. Zhu, Z. Fan, X. Li, and W. Wu, "Structural Optimization Design and Strength Test Research of Connecting Rod Assembly of High-Power Low-Speed Diesel Engine," *Machines*, vol. 10, no. 9, Sep. 2022, Art. no. 815, https://doi.org/10.3390/machines 10090815.

[13] Otai Special Steel. "S50C Carbon Steel - JIS G4051 S50C steel plate." https://www.otaisteel.com/s50c-carbon-steel/.

[14] V. Msomi and S. Mabuwa, "Analyzing the Influence of Microstructure on the Mechanical Properties of TIG Welded Joints processed by Friction Stir considering the sampling Orientation," *Engineering, Technology & Applied Science Research*, vol. 14, no. 1, pp. 12470–12475, Feb. 2024, https://doi.org/10.48084/etasr.6459.

[15] A. B. Sidhpara, V. I. Kureshi, P. A. Patel, "Comparision of Manufacturing Methods and Analysis of Connecting Rod for Reducing Cost," *International Journal of Engineering Research & Technology*, vol. 2, no. 5, pp. 1516-1523, May. 2013.

[16] S. S Gandhul, V. Surywanshi, A. Kumar Shriwastava, "Calculation Methodology for Design of Connecting Rod Considering Fatigue in IC Engine," *International Journal of Engineering Applied Sciences and Technology*. vol. 4, no. 10, pp. 116-121, Feb. 2020.

[17] A. Muhammad, I. H. Shanono, "Static Analysis and Optimization of a Connecting Rod, " *International Journal of Engineering Technology and Sciences*. vol. 6, no. 1, pp. 24-40, Jun. 2019, http://doi.org/10.15282/ijets.6.1.2019.1003.

[18] B. Inseemeesak and V. Boonmag, "Failure Analysis of S55C Medium Carbon Steel for the Pickup Crankshaft," *International Journal of Mechanical Engineering and Robotics Research*, vol. 13, no. 1, pp. 175–183, 2024, https://doi.org/10.18178/ijmerr.13.1.175-183.

[19] M. Kumar and S. N. Prajapati, "Design, Buckling and Fatigue Failure Analysis of Connecting Rod: A Review," *International Journal of Advanced Engineering Research and Science*, vol. 4, no. 7, pp. 39–44, 2017, https://doi.org/10.22161/ijaers.4.7.7.

[20] B. A. Vinayakrao, M. C. Swami, "Analysis and Optimization of Connecting Rod used in Heavy Commercial Vehicles," *International Journal of Engineering Development and Research*, vol. 5, no. 3, pp. 684-707, Aug. 2017.

[21] R. Shrivastava, "Finite Element Analysis of Connecting Rod for Two-Wheeler and Optimization of Suitable Material Under Static Load Condition," *International Research Journal of Engineering and Technology*. vol. 4, no. 2, pp. 537-543, Feb. 2017.

[22] I. Ismail, E. Abdelrazek, M. Ismail, and A. Emara, "Enhancing the Durability of Connecting Rod of a Heavy-Duty Diesel Engine," *International Journal of Automotive and Mechanical Engineering*, vol. 18, no. 2, Jun. 2021, https://doi.org/10.15282/ijame.18.2.2021.10.0666.

[23] W. M. K. Helal, Z. Wenping, L. Xiaobo, W. Guixin, S. Yanpan, and C. Guangku, "Analysis of Low-Speed Diesel Engine Connecting Rod Made of AL360," *Journal of Physics: Conference Series*, vol. 1939, no. 1, May 2021, Art. no. 012023, https://doi.org/10.1088/1742-6596/1939/1/012023.

[24] J. A. Martins and E. C. Romao, "Fracture Analysis of a Cycloidal Gearbox as a Yaw Drive on a Wind Turbine," *Engineering, Technology & Applied Science Research*, vol. 14, no. 1, pp. 12640–12645, Feb. 2024, https://doi.org/10.48084/etasr.6613.

[25] N. Pervan, M. Trobradovic, A. J. Muminovic, H. Lulic, S. Metovic, and V. Hadziabdic, "Effects of Geometry Design Parameters on the Fatigue Failure of a Drive Axle Housing using Finite Element Analysis," *Engineering, Technology & Applied Science Research*, vol. 14, no. 1, pp. 12567–12573, Feb. 2024, https://doi.org/10.48084/etasr.6467.